Numerical modelling of the damage modes in UD thin carbon/glass hybrid laminates

Meisam Jalalvand[*,1], Gergely Czél[†], Michael R. Wisnom[‡]

Advanced Composites Centre for Innovation and Science, University of Bristol, Bristol, UK
[*]M.Jalalvand@bristol.ac.uk
[†] G.Czel@bristol.ac.uk
[‡] M.Wisnom@bristol.ac.uk

Abstract

This paper proposes a new FE-based approach for modelling all of the possible damage modes in glass/carbon UD hybrid laminates in tensile loading. The damage development is modelled by two sets of cohesive elements, (i) periodically embedded in the carbon layer for modelling carbon fibre failure and (ii) at the glass/carbon interface to capture delamination. The analysis is stopped when the glass layer failure is predicted by integrating the stress distribution over the glass layer to calculate an equivalent stress for unit volume of the glass. The proposed method is validated against the experimental results and then used to simulate the progressive damage process of other hybrid configurations and finally produce a damage-mode map for this material set. The method can easily be applied to other hybrids to assess their performance by producing damage-mode maps.

Keywords:

A. Hybrid composites; B. Delamination; B. Failure; C. Finite Element Analysis; Thin-ply layer

[1] Corresponding author

1. Introduction

Lack of ductility in composite materials is one of their main drawbacks. The brittle failure means that usually the fracture of fibrous composites happens suddenly without any warning and the chance of finding damage before it becomes critical is low. As a result, large values of safety factor are necessary, reducing the weight saving potential.

Hybridisation of different continuous uni-directional (UD) prepregs is one of the successful approaches to address the issue of lack of ductility. Hybrids are usually made up of two different types of fibres and in many of the previous studies, carbon and glass layers were the constituents[1–5]. Since the failure strain of carbon fibres is lower than glass fibres, the first damage is certainly in the carbon layer but the final failure of the specimen depends on other material properties, interface toughness and the thickness of the layers.

While most of the previous works on hybridisation were concentrating on the enhancement of the carbon failure strain [6], Czél and Wisnom [7] tried to produce gradual failure and pseudo-ductile responses. They showed that if the carbon layer in a glass/carbon hybrid is thin enough, catastrophic delamination propagation around the first carbon failure is suppressed and therefore further failures in the carbon layer may occur. If the load is increased and the glass layer is not broken, it has been shown that the fragmented carbon layer may start to pull out stably from the cracks. All of these proposed failure mechanisms happen gradually, introducing pseudo-ductility into the stress-strain curve.

Study of UD hybrids is helpful to understand the mechanisms which have introduced pseudo-ductility in their response. This knowledge can then be applied in designing more general lay-ups with gradual failure.

The few proposed hybrid analyses were mainly concentrated on the prediction of hybrid strength. Based on the Weibull random distribution of the constituent fibres' strength, Zweben proposed an idealised model to study the failure strain of a hybrid laminate [8] but the obtained results agreed only qualitatively with the experiments. Another approach for predicting the hybrid strength has been proposed by Manders and Bader[1]. Using a simple schematic graph, they tried to relate the strength of glass/carbon hybrid to the carbon ratio. The proposed method was based on a simple 1D equation considering no delamination or stress concentration. Wu also did some numerical macro scale analyses considering a nonlinear material response and ignoring any permanent deformation [9]. A softening material response was applied to model the rupture of the high-modulus carbon layer. The model was able to show qualitatively the effect of the different ratios and the load drops.

The proposed approaches were mainly for investigating the strength of different hybrids rather than trying to study the response of the hybrid during damage progression. The available approaches have generally not considered delamination propagation or stress concentrations but were rather based on fibre failures of the carbon, glass and their interaction.

Since the aim of this paper is to study the pseudo-ductility introduced by hybridisation, a new approach for modelling the damage process of the UD sandwich hybrid composites is proposed which in contrast to previous approaches is able to deal with all the observed failure modes. The advantage of such a modelling approach is that it can then be used for more investigations of the hybrid behaviours with fewer restrictions e.g. on material properties and ply-thicknesses. A novel damage mode map is proposed that shows how the failure depends on the absolute and relative thickness of carbon, which is useful in understanding the relative effect of these factors and in designing new hybrid configurations.

1.1. Experimental results

Czél and Wisnom [7] have performed a series of tensile tests on different combinations of UD thin carbon and standard thickness glass prepregs of: [$G_2/C_m/G_2$] (m=1-4) where C and G indicate SkyFlex USN020A carbon and Hexcel 913/E-Glass prepreg layers with the approximate measured thickness of 0.030 mm and 0.144 mm respectively.

Two additional series of [$G/C_n/G$] (n=1, 2) type specimens of the same materials were tested, both being scaled versions of other types presented in [7] to cover the whole range of damage scenarios. Figure 2 shows the stress-extension curves of all the tested specimens. It is obvious from the Figure 1 (a-b) that both specimen types showed a sudden failure close to the strain to failure of the carbon fibres, however the [G/C/G] type specimens failed at significantly higher extensions. The main difference compared to the specimens tested earlier [7] was, that the glass plies failed very shortly after the first few carbon layer fractures.

Before any damage in the hybrids, the strain in the carbon and glass layers is equal and uniform all over the specimen. Therefore, there is no shear at the interface or stress variation along the length of the specimen. Since the failure strain of the carbon layer is lower than glass, the first damage in all of the hybrid laminates is the breakage of the carbon layer. However, the thickness of the carbon and glass layers determines the following damage mechanisms. A summary of the observed damage modes after the first discrete damage of the carbon layer in the different laminates in addition to the final glass failure strain is given in Table 1. In some of the laminates, especially with thinner carbon layers, the damage process is followed by carbon layer fragmentation, but in laminates with 3 or more carbon layers, it is only followed

by delamination at the carbon-glass interface. In the laminate [$G_2/C_2/G_2$], after discrete cracking in the carbon layer (carbon layer fragmentation), interlaminar cracks initiated causing more gradual failure. Since the interlaminar cracks were spread over the whole specimen and grew gradually, this mechanism is called dispersed delamination in Table 1.

2. Modelling approach

To model the behaviour of the UD glass and carbon layers, a 2-D finite element analysis of a section through the laminate has been performed using quadratic quadrilateral elements with linear elastic material properties. Due to symmetry of all of the laminates about the mid-plane, just half of the specimen is modelled. Such a symmetric condition is valid since it was observed that carbon fibre fragmentation and also delamination propagation occurred approximately symmetrically about the mid-plane. Judging the validity of the symmetry assumption for the glass fibre failure is difficult in the performed experiments, but the symmetry assumption remains sound up to the prediction of first fibre failure of the glass layer, when the whole analysis is stopped.

Two main progressive damage modes of carbon layer fragmentation and delamination are modelled together with initiation of glass fibre failure. Cohesive elements are used here for modelling both of the progressive damage modes to capture the interaction of in-plane and interlaminar damage modes properly. A row of cohesive elements is placed at the glass/carbon interface for modelling the delamination. A pure mode-II criterion has been used since delamination is due to shear stresses with some compression at the crack tip. A bilinear cohesive law based on the formulation of [10] with no permanent deformation in the unloading path is used for the cohesive elements.

The probability of glass fibre failure, *P*, is calculated from Equation (1) which is based on the Weibull statistical distribution for failure of brittle materials, and has been found to represent the behaviour of unidirectional glass-epoxy quite well [11]. The distribution of stress along the fibre direction $\sigma_1(x,y)$ over the whole volume of the specimen, *V*, determines when the glass fibres are likely to break. The characteristic strength, σ_1^0, and Weibull modulus, *m*, are the two material constants in this approach by which the size effect is taken into account for a certain material.

$$p = \exp\left(-\int_V \left(\frac{\sigma_1(x,y)}{\sigma_1^0}\right)^m dV\right) \tag{1}$$

It is possible to relate the actual varying stress distribution $\sigma_1(x,y)$ to an equivalent constant longitudinal stress in a unit volume of the glass layer with equal probability of failure, σ_{eq}, as given in Equation (**2**), thereby taking both the size effect and stress concentration into account.

$$\sigma_{eq} = \sqrt[m]{\int_V (\sigma_1(x,y))^m dV} \tag{2}$$

For calculating σ_{eq} in the FE, the value of stress in the fibre direction at the integration points, $\sigma_1^{i,j}(x,y)$, is added up over all of the elements in the models:

$$\sigma_{eq} = \sqrt[m]{\sum_{i=1}^{\text{no.elem.}} \sum_{j=1}^{\text{no.int.point.}} (\sigma_1^{i,j}(x,y))^m w_j V_i} \tag{3}$$

Where the indices *i* and *j* represent the different number of elements and integration points respectively and also V_i and w_j are their corresponding volume and weight.

It is worth mentioning that only the point of first glass fibre failure is predicted here rather than progressive damage. This is because when the glass fibre failure initiates, the damage localises and the composite fails quickly. Progressive modelling of glass failure is therefore not very interesting and the emphasis of this paper is on the non-linear response before initiation of glass fibre failure.

The mechanical properties of the Hexcel 913/E-Glass were assumed as E_1=38.7 GPa, E_2= 15.4 GPa, G12=4.34 and ν_{12}=0.3 according to [12]. The value of E_1 of Hexcel 913/E-glass which was measured as 43.9 GPa for 0.127 mm nominal ply thickness in [12] was corrected for the measured thickness of the glass layer which was 0.144 mm in the hybrid combination, reflecting the lower fibre volume fraction in the thicker plies. The mechanical properties of SkyFlex USN020A carbon layer were assumed as E_1=101.7 GPa, E_2= 6.0 GPa, G_{12}=2.4 and ν_{12}=0.3 according to [13]. Separate tests have been performed on UD hybrid laminates of [G_2/C_4/G_2] with a central cut in the carbon layers and the value of G_{IIc} for the interface between these two different prepregs was found to be 1.0 N/mm using the procedure introduced in [14]. The shear strength of the cohesive elements was assumed 67 MPa based on the ±45 shear test results [13].

According to [7], the highest thermal residual strain due to the cure process is less than 3% of the failure strain of the carbon layer in the [G_2/C/G_2] laminate. This is because the laminates are all UD and the mismatch between the fibre thermal expansions is not significant. Since the damage process of the hybrids is dominated by fibre rather than matrix failure, residual stresses are not considered in this study.

2.1. Local damage analysis

To study the interaction of delamination and glass fibre failure, a quarter of the hybrid specimen with 4mm length was modelled including an open central crack in the carbon layer representing the first damage (Figure 2). The glass and carbon layers were meshed with quadratic quadrilateral elements and the elastic properties mentioned in the previous section. Modelling with this approach is straight forward and due to the size of the model, fine elements can be used. Therefore, this approach is suitable for investigating the stress concentration in the glass layer around the fragmented carbon layer. There are certain similarities with [15] in which the interaction of matrix cracking and delamination has been studied in cross-ply laminates. The transverse crack was assumed open and the delamination propagation modelled using cohesive elements. However, the fibre failure prediction of the outer layers was not considered there.

2.2. The full response

The full response of the specimen cannot be obtained with the previous method since the carbon fragmentation is not modelled progressively. Such a method is also incapable of giving any information about the crack spacing in the fragmented carbon layer or when the damage mode changes from carbon fragmentation to delamination or glass failure. Furthermore, the length of the model (2mm) is not much longer than the interfacial damage process zone, so during the load application and while damage is growing around the fragmented carbon layer at the interface, the longitudinal stiffness of the model reduces. On the other hand, the elongation of the specimen was globally measured over 120 mm in the experiments, so it is not possible to directly match the strains obtained from the previous approach with the experimentally measured extensions.

To overcome these shortcomings, a longer model (50 mm), more representative of the whole specimen, was used, with embedded cohesive elements in the carbon layer to model the carbon fragmentation. This length of the model is adequate to capture enough cracks in the carbon layer to represent the progressive damage modes in the experiments.

Figure 3 shows schematically the model and also the element arrangement over 0.25mm of this model.

Before damage initiation, the embedded cohesive elements in the carbon layer behave elastically, and it is important to make sure they do not significantly affect the response. The stiffness of the carbon layer with embedded cohesive element, E'_{1C}, according to [16] is related

to the modulus of the carbon layer in the fibre direction, E_{1C}, and the elastic stiffness of the cohesive elements, *K*, as equation (4).

$$\frac{E'_{1C}}{E_{1C}} = \frac{1}{1+\frac{n-1}{L}\frac{E_{1C}}{K}} \quad \textbf{(4)}$$

where *n* is the total number of cohesive element rows in the carbon layer and *L* is the total length of the model which is 50 mm here. To keep the contribution of cohesive elements in the elastic stiffness of the carbon layer negligible, it is necessary to keep $\frac{n-1}{L}\frac{E_{1C}}{K}$ as small as possible by selecting a large enough value for *K*. According to the material properties and stated geometry, a value of $K=10^9$ N/mm^3 limits the stiffness reduction of the carbon layer to less than 0.08%. The cohesive elements at the glass/carbon interface do not affect the stiffness of the laminate greatly, so their penalty stiffness can be assumed similar to the ordinary cohesive elements applied for crack propagation modelling. Here, a value of $K=10^5$ N/mm^3 is sufficient. The strength of the embedded cohesive elements in the carbon layer determines the strength of the carbon layer and it is given a random variation over the length of the specimen to represent the material variability and avoid simultaneous damage initiation in all of the cohesive elements. According to the experimental results[7], the first fibre failure in the carbon layer is observed at a strain of around 1.93% on average, which means that the initial strength of the carbon layer for this volume fraction of material is equal to 1962MPa.

A random distribution obtained from (5) and based on a Weibull distribution [17] is assigned to the cohesive elements inside the carbon layer.

$$T = T^0\left[\ln\left(\frac{1}{1-\eta}\right)\right]^{\frac{1}{m}} \quad \textbf{(5)}$$

Where η is a random variable between 0 and 1. Using the Weibull modulus of m=41 typical for carbon fibres [18] and scale factor of T^0=2339 MPa, the obtained distribution shown in Figure 4 gives a minimum value of 1957 MPa, which is close to the observed first failure of the carbon layer. Obviously, such a strength distribution is not unique but since the minimum value in the distribution is very close to the strength of the carbon, it was appropriate for the modelling in this approach.

3. Numerical results

All of the modelling work in this paper was performed with an in-house implicit FE code which was validated and used in several works[16,19,20]. To prevent divergence, especially for the

cases with catastrophic delamination propagation, the modified secant method (stiffness matrix of the structure during unloading) was used. This increased the number of iterations needed but guaranteed the convergence, even with sharp load drops.

3.1. Local damage analysis

The results presented in this part were obtained with the modelling approach presented in section 2.1 to investigate the interaction of the two damage modes of delamination and glass fibre failure. According to Table 1, the glass fibre failure in the two laminates [G/C/G] and [$G_2/C_2/G_2$] with similar glass/carbon ratio is different. To investigate this issue, delamination initiation and propagation of these laminates was analysed in the model with an initial crack in the carbon layer and a cohesive element row at the glass/carbon interface. Both geometry and mesh schemes were scaled up by the factor of 2 to maintain everything similar, so the length of the specimens [G/C/G] and [$G_2/C_2/G_2$] were assumed 2 mm and 4 mm respectively. In the absence of entities with nonlinear properties, the stress distribution in both models should be identical, however, using cohesive elements with interlaminar damage can make the stress distribution around the fragmented carbon layer different. Figure 5 indicates the contours of longitudinal stress, σ_x, around the fractured carbon layer in the two laminates [G/C/G] and [$G_2/C_2/G_2$] before delamination propagation at an extension of 2.4%. Obviously, the stress gradient in the carbon layer is higher in the thinner laminate and therefore the damage process zone is shorter which causes higher stress concentrations around the fragmented carbon layer. However, the process zone in the thicker specimen is longer, thus the stress concentration is lower. The more even stress distribution over the specimen means a lower value of σ_{eq} for the glass fibres and therefore lower risk of glass fibre failure for the thicker case. Figure 6 indicates the variation of σ_{eq} versus applied displacement. At small loads, the cohesive elements are mainly in the linear elastic region, therefore σ_{eq} in both the laminates is the same. However at larger loads, the stress concentration is supressed in the thicker laminate due to greater interlaminar damage growth and therefore, the glass failure probability increases more slowly. The slightly higher value of σ_{eq} in [$G_2/C_2/G_2$] laminates at small loads is due to the larger volume of the glass layer in this laminate.

To investigate the effect of mesh refinement on the predicted glass fibre failure, two models with similar lengths of 2mm and layup of [$G_2/C_2/G_2$] but different element sizes were compared. The model with the fine mesh scheme has 3400 elements with element size around the interface of 7×10 μm, and the coarse model has a total of 360 elements with elements sized 16×50 μm around the interface. Figure 7 shows the obtained σ_{eq} from these two mesh schemes.

The predicted σ_{eq} of the model with the fine mesh is larger at small extensions when the interlaminar damage around the fragmented carbon layer has not developed significantly and the results are dominated by the elastic response of the layers. However at extensions of about 1.8% and more, they are coincident, showing that the predicted glass failure is not sensitive to the mesh scheme as long as it happens in this range of strain where the damaged cohesive elements at the interface have suppressed the stress concentration around the fragmented carbon layer. In other words, the stress concentration at large values of strain is mainly controlled by the cohesive damage rule, and mesh size does not affect it significantly.

3.2. The full response

The previous approach in section 2.1 is good for studying the interaction of delamination and glass failure, but is not suitable to model the full response of the laminates and to compare with experimental results. To model the whole damage process, the approach described in section 2.2 is used. The applied mesh is similar to the coarse mesh, which was shown to be adequate as long as the glass failure happens at sufficiently high strains. To avoid any simultaneous damage initiation in the neighbouring embedded cohesive elements for modelling the carbon fragmentation, small steps with a constant extension of 0.01% per step were applied in displacement-control.

Due to the uniform stress distribution over the specimen before damage initiation, the first carbon layer fragmentation is the same in all of the specimens but after that, the number of carbon and glass layers determines the following damage modes. The analysis continues until the prediction of glass failure when the criterion of "$\sigma_{eq} \geq 1350$ MPa" is satisfied. This value of equivalent stress of the glass layers was chosen as it gives a good agreement with the experimental results. Figure 8 indicates the variation of σ_{eq} for different layups versus extension up to their final failure point which is in bold. Up to the first carbon layer fragmentation, there is only a small difference between the laminates because of the different glass volume. However, the stress concentration and interlaminar damage distribution make the growth of σ_{eq} different after carbon layer fragmentation. The big jump in the value of σ_{eq} in the laminate [G/C_2/G] causes an early glass failure after the first carbon layer fragmentation. The rise of σ_{eq} in the other laminates is more gradual after a smaller jump and in some cases other damage (i.e. delamination) can grow until the prediction of glass fibre failure. The laminates [G/C/G], [G_2/C_2/G_2] and [G_2/C/G_2] have some more carbon layer fragmentation randomly spread over their length before the glass failure. The final failure of the laminates [G_2/C_3/G_2] and [G_2/C_4/G_2]

does not happen before delamination is complete. All of the predicted damage modes in each laminate are in agreement with the observed experimental behaviour [7].

Figure 10 (a-f) indicates the obtained stress-extension curves of the different laminates (black line with a bold dot at the end) against the experimental results (grey lines). The early glass failure of the laminates with one single glass layer on each side is well predicted in the FE results. In the laminates [G_2/C/G_2] and [G_2/C_2/G_2], a stress deviation from the linear elastic response is distinguishable in both experimental and numerical results before glass failure. In the laminates with 3 and 4 central carbon layers, there is a load drop after the first carbon layer failure due to rapid initial delamination propagation. The delamination propagation then becomes stable and since the value of G_{IIc} of the interface is assumed constant, the load stays constant until the delamination extends over the whole glass/carbon interface. Glass fibre failure then happens when the delamination is complete and the load is only carried by the glass layers in these two laminates. As mentioned in section 2, only the point of first glass fibre failure is predicted (the progressive damage was not modelled) and therefore, the load drops during glass fibre failure were not captured in the analysis.

Table 2 gives the numerical results of all of the modelled laminates in this paper including both tested and a number of additional non-tested specimens. The tested specimens are specified by their layup configuration which is mentioned in the first column of the table. The damage modes are mentioned in the order they were observed in the numerical modelling and the predicted glass failure strain and also the difference from the experimental results are given in the last column for the tested specimen. The predicted glass failure of the tested specimens is less than 5% different from the average measured glass failure in the experiments, except the one for the laminate [G_2/C/G_2]. The glass failure in this laminate has been predicted 11.5% earlier. It is believed that this difference is mainly because of non-uniformity of the carbon fragmentation across the width, which particularly affected this laminate. The proposed two-dimensional FE approach assumes that all of the tips of the fragmented carbon layer are aligned across the width, so the stress concentration is higher and glass failure is predicted earlier. In this respect the proposed approach is conservative.

Figure 9 indicates the contours of stress in the fibre direction in the [G_2/C/G_2] and [G_2/C_2/G_2] laminates between first carbon layer fragmentation and final glass failure. Around the fragmented carbon layer, the stress drops in the carbon layer at the middle and increases in the glass layer. Due to the shorter process zone around the fragmented fibres in the thinner laminate, the crack density is also higher in this laminate. The average crack spacing of these

two laminates is 1.0 and 0.3 mm^{-1} over the 50mm length of the model which is in agreement with the experimental observations.

The unstable delamination after carbon layer fragmentation of the laminate [$G_2/C_3/G_2$] is shown in Figure 11. In fact, the sudden load drop in Figure 10 (e) is due to this unstable partial delamination of the specimen.

4. Damage mode domain maps

After validating the modelling approach with the experimental results, other new hybrid combinations can be analysed with the same numerical tool. To investigate the variation of damage modes with respect to the glass and carbon layer thicknesses, new hybrid combinations as indicated in the Table 2 were modelled. The material properties and the strength distribution of the embedded cohesive elements were the same as in the previously modelled specimens. The only difference between all of these new models and the previous ones is that the variation of glass and carbon layer thickness was not constrained by the ply thickness. Therefore, the number of possible hybrid configurations is increased which is helpful in distinguishing the dependency of the damage process on the geometry of the hybrid. The damage modes after first carbon fragmentation along with the glass failure strain obtained from the proposed approach are also included in Table 2.

Figure 12 shows all of the analysed hybrid specimens on a chart showing the absolute and relative thickness of the carbon layers. Each point on the graph relates to a specific hybrid configuration and from the damage modes obtained from the model, different areas have been associated with different damage processes and divided schematically. The experimentally tested configurations are also distinguished with an additional bigger square marker. With such a plot, it is possible to predict the damage modes of a particular hybrid or to design a hybrid for a certain desired characteristic. To increase the pseudo-ductile part of the stress-strain response, it is necessary to avoid single delamination and premature glass layer failure. Additionally, it is important to increase the carbon proportion to increase the potential of larger stiffness variation during the damage process. But to have both carbon fragmentation and diffuse delamination in the damage process, an upper limit exists for the carbon ratio. Furthermore, there are lower and upper bands on the carbon thickness in laminates with the same carbon ratio to achieve the desired diffuse delamination. This map can also be produced for other material combinations and used to help to design hybrid laminates with the desired damage process and characteristics.

5. Conclusion

In this paper, two modelling approaches for the damage process of UD hybrid laminates have been discussed. In the first approach, the interaction of delamination and glass fibre failure was examined and it was shown that the difference in glass fibre failure of the scaled laminates of [G/C/G] and [G_2/C_2/G_2] is due to the different stress concentration. In the thicker laminate, the process zone is longer and therefore the stress distribution in the glass layers is more uniform but in the thinner laminate the interface is less damaged so the stress concentration is higher and therefore the glass fails earlier.

The second approach analyses the full damage process including carbon fragmentation, delamination and glass fibre failure. Cohesive elements with a random distribution of strength were embedded to represent carbon layer fragmentation and another row of cohesive elements between the glass and carbon layers was included for modelling of delamination. The obtained progressive damage results in all of the laminates were in agreement with the experimental observations. The crack spacing in the carbon layer was also properly modelled in this approach. The obtained FE stress-extension curves were compared against the experimental results which showed the capability of the proposed approach to simulate the observed behaviour. The largest difference between the FE results and experiments was in the prediction of the glass failure strain for the laminate [G_2/C/G_2] which is believed to be due to variation of carbon fragmentation across the width.

Finally, the validated approach was used to model other new hybrid configurations. All of the analysed specimens then were categorised into four different groups. They were also depicted on a chart with the axes of absolute and relative carbon thickness. This graph clearly indicates that there are upper bounds on the maximum carbon ratio to avoid premature glass failure and single delamination. Such a damage mode map is very helpful for designing new hybrid configurations with other materials.

Acknowledgement

This work was funded under the EPSRC Programme Grant EP/I02946X/1 on High Performance Ductile Composite Technology in collaboration with Imperial College, London.

References

[1] Manders PW, Bader MG. The strength of hybrid glass/carbon fibre composites. J Mater Sci 1981;16:2233–45.

[2] Summerscales J, Short D. Carbon fibre and glass fibre hybrid reinforced plastics. Composites 1978;9:157–66.

[3] Bunsell AR, Harris B. Hybrid carbon and glass fibre composites. Composites 1974;5:157–64.

[4] Aveston J, Sillwood JM. Synergistic fibre strengthening in hybrid composites. J Mater Sci 1976;11:1877–83.

[5] Chamis CC, Lark RF, Sinclair JH. Mechanical property characterization of interply hybrid composites. Am. Soc. Test. Mater. Symp., Dearborn, Michigan: 1979.

[6] Kretsis G. A review of the tensile , compressive , flexural and shear properties of hybrid fibre- reinforced plastics. Composites 1987;18:13–23.

[7] Czél G, Wisnom MR. Demonstration of pseudo-ductility in high performance glass-epoxy composites by hybridisation with thin-ply carbon prepreg. Compos Part A Appl Sci Manuf 2013;52:23–30.

[8] Zweben C. Tensile strength of hybrid composites. J Mater Sci 1977;12:1335–7.

[9] Wu ZS. Structural strengthening and integrity with hybrid FRP composites. Proc. 2nd Int. Conf. FRP Compos. Civ. Eng. 2004, Aust. Keynote Lect., 2004, p. 93–105.

[10] Camanho PP, Davila CG, Moura MF De. Numerical simulation of mixed-mode progressive delamination in composite materials. J Compos Mater 2003;37:1415–38.

[11] Wisnom MR, Atkinson JW. Reduction in tensile and flexural strength of unidirectional glass fibre-epoxy with increasing specimen size. Compos Struct 1997;38:405–11.

[12] Hallett SR. Numerical Investigation of Progressive Damage and the Effect of Layup in Notched Tensile Tests. J Compos Mater 2005;40:1229–45.

[13] Fuller J, Wisnom MR. Damage suppression in thin ply angle-ply carbon/epoxy laminates. 19th Int. Conf. Compos. Mater., Montreal: 2013.

[14] Cui W, Wisnom MR, Jones M. An Experimental and Analytical Study of Delamination of Unidirectional Specimens with Cut Central Plies. J Reinf Plast Compos 1994;13:722–39.

[15] Khokhar ZR, Ashcroft I a., Silberschmidt V V. Interaction of Matrix Cracking and Delamination in Cross-ply Laminates: Simulations with Stochastic Cohesive Zone Elements. Appl Compos Mater 2011;18:3–16.

[16] Jalalvand M, Hosseini-Toudeshky H, Mohammadi B. Numerical modeling of diffuse transverse cracks and induced delamination using cohesive elements. Proc Inst Mech Eng Part C J Mech Eng Sci 2012;227:1392–405.

[17] Okabe T, Nishikawa M, Takeda N. Numerical modeling of progressive damage in fiber reinforced plastic cross-ply laminates. Compos Sci Technol 2008;68:2282–9.

[18] Wisnom MR. Relationship between strength variability and size effect in unidirectional carbon fibre / epoxy. Composites 1991;22:47–52.

[19] Jalalvand M. Modeling the Effects of Delamination Induced by Matrix Cracking using Multiscale Damage Mechanics (PhD thesis). Amirkabir University of Technology, 2013.

[20] Jalalvand M, Hosseini-Toudeshky H, Mohammadi B. Homogenization of diffuse delamination in composite laminates. Compos Struct 2013;100:113–20.

Tables

Table 1- Damage modes after first carbon layer breakage and glass failure strain

Lay-up	Damage modes after first fragmentation of carbon layer			Glass failure strain (%)
	1st	2nd	3rd	
[G/C/G]	Carbon fragmentation	Glass failure		2.13
[G/C_2/G]	Glass failure			1.93
[G_2/C/G_2] *	Carbon fragmentation	Glass failure		2.62
[G_2/C_2/G_2] *	Carbon fragmentation	Dispersed delamination	Glass failure	2.24
[G_2/C_3/G_2] *	Single delamination	Glass failure		2.75
[G_2/C_4/G_2] *	Single delamination	Glass failure		2.75

* From reference [7].

Table 2- The analysed hybrid combinations, their damage modes and glass failure strain

Carbon thickness (mm) [tested layup]	Carbon thickness, proportion of total	Damage modes after first carbon breakage			Predicted glass failure strain [error]
		1	2	3	
0.020	0.17	Carbon fragmentation	Glass failure		2.04
0.020	0.20	Glass failure			1.96
0.03 [G/C/G]	0.09	Carbon fragmentation	Glass failure		2.19 [2.8%]
0.03 [G_2/C/G_2]	0.05	Carbon fragmentation	Glass failure		2.32 [11.5%]
0.040	0.15	Carbon fragmentation	Glass failure		2.04
0.040	0.20	Glass failure			1.93
0.050	0.10	Carbon fragmentation	Glass failure		2.21
0.050	0.15	Carbon fragmentation	Glass failure		2.07
0.06 [G/C_2/G]	0.17	Glass failure			2.02 [4.7%]
0.06 [G_2/C_2/G_2]	0.09	Carbon fragmentation	Diffuse delamination	Glass failure	2.31 [3.1%]
0.064	0.18	Glass failure			2.00
0.066	0.13	Carbon fragmentation	Diffuse delamination	Glass failure	2.20
0.070	0.11	Carbon fragmentation	Diffuse delamination	Glass failure	2.48
0.070	0.19	Glass failure			1.94
0.076	0.12	Carbon fragmentation	Diffuse delamination	Glass failure	2.61
0.076	0.15	Single delamination	Glass failure		2.40
0.080	0.22	Glass failure			1.93
0.09 [G_2/C_3/G_2]	0.13	Single delamination	Glass failure		2.65 [3.6%]
0.090	0.17	Single delamination	Glass failure		2.65
0.12 [G_2/C_4/G_2]	0.17	Single delamination	Glass failure		2.65 [3.6%]

Figures

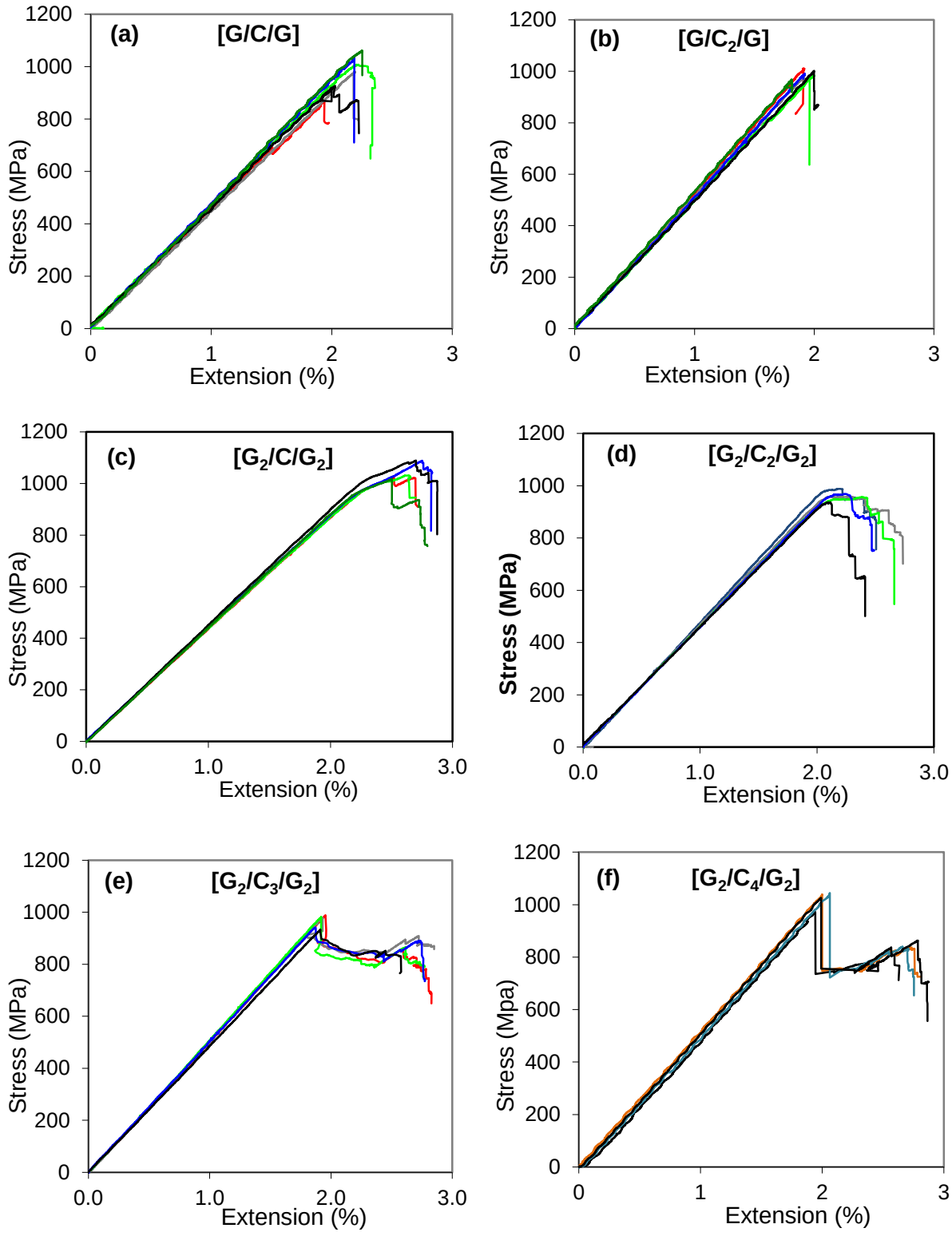

Figure 1- Stress-extension response of the new (a-b) and previously [7] tested (c-f) specimen

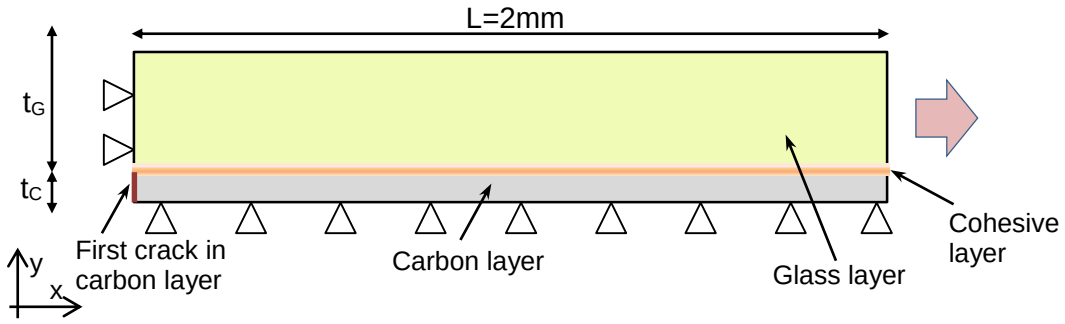

Figure 2- First approach for local damage analysis to study of delamination and glass failure

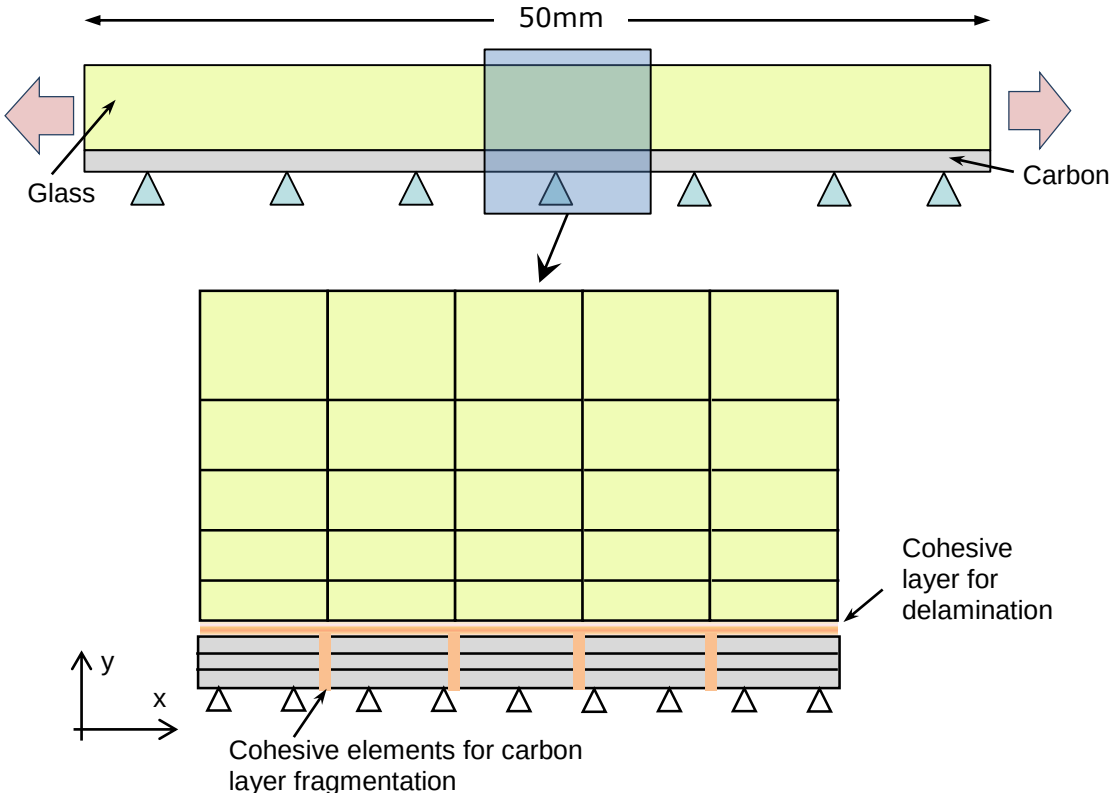

Figure 3- Modelling the full response of the hybrid laminates

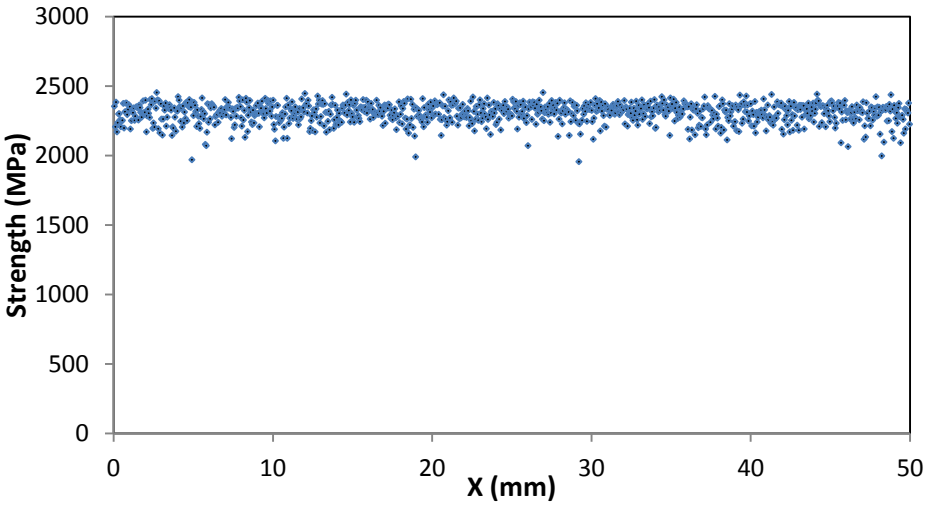

Figure 4- The distribution of cohesive element rows over the length of the model

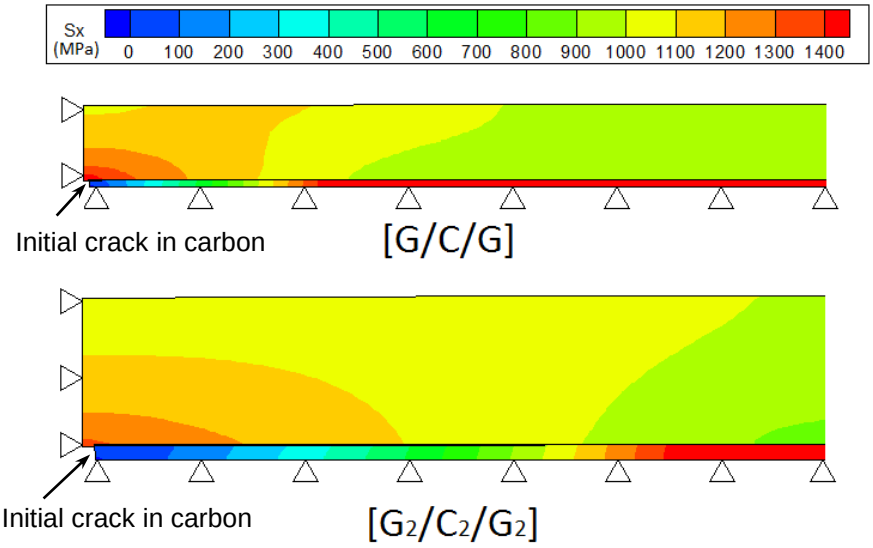

Figure 5-Contour of stress in fibre direction around the fragmented carbon layer

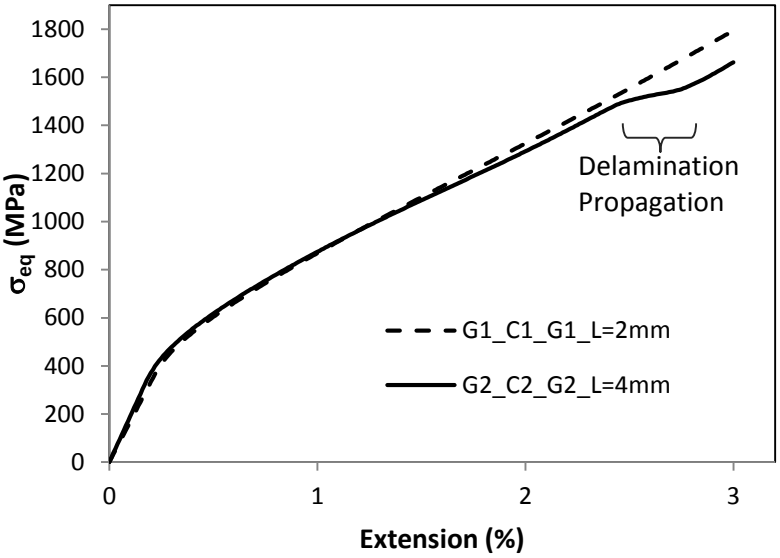

Figure 6- σ_{eq} of glass layer in [G/C/G] and [$G_2/C_2/G_2$] laminates

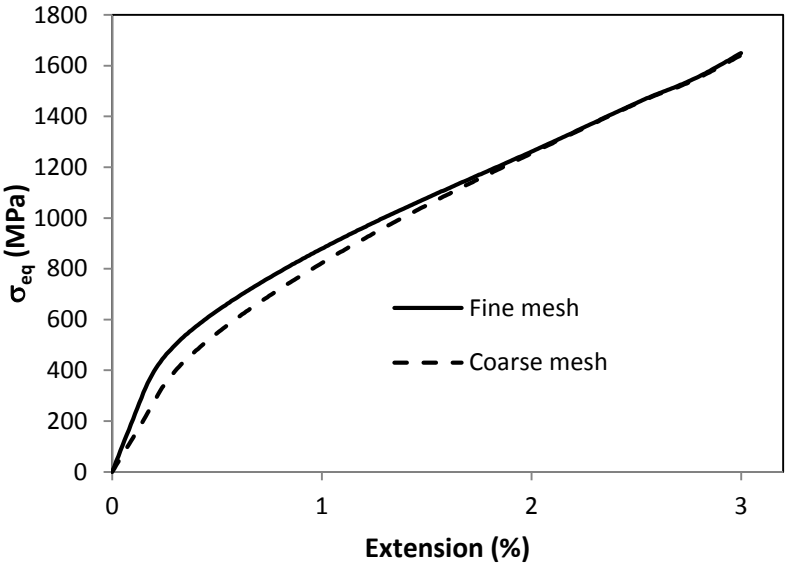

Figure 7- σ_{eq} for [$G_2/C_2/G_2$] from fine and coarse mesh schemes

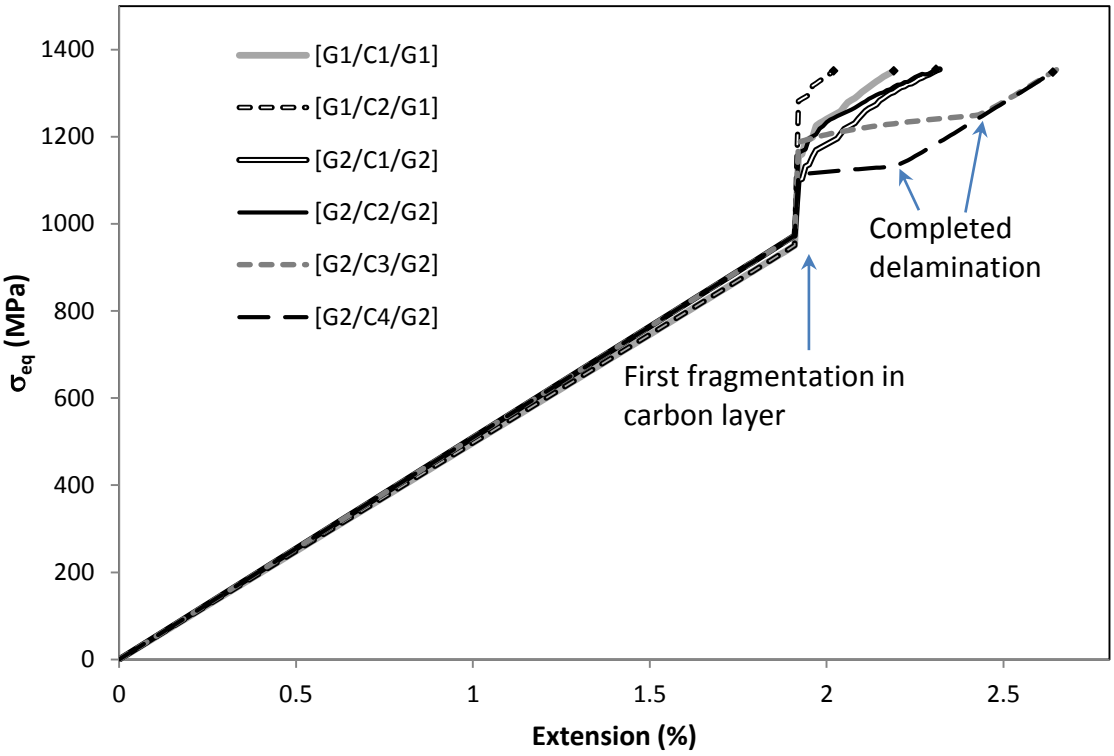

Figure 8- σ_{eq} of different layups up to the predicted glass failure

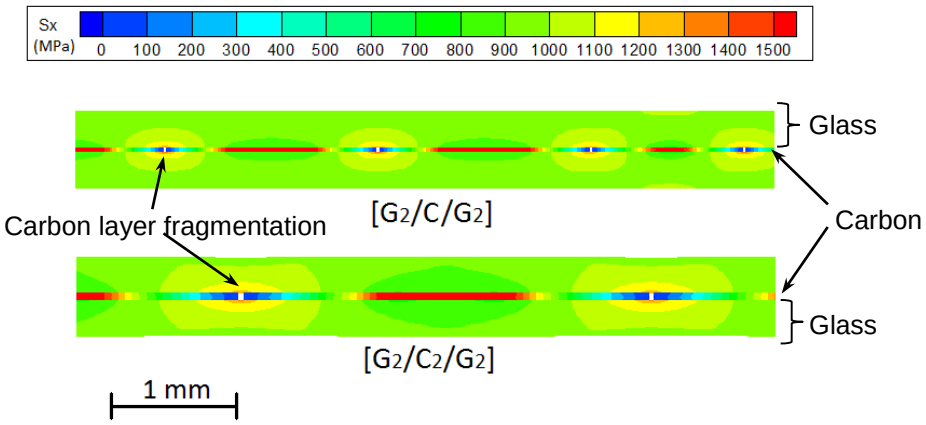

Figure 9- Contour of stress in fibre direction in laminates [G/C/G] and [$G_2/C_2/G_2$]

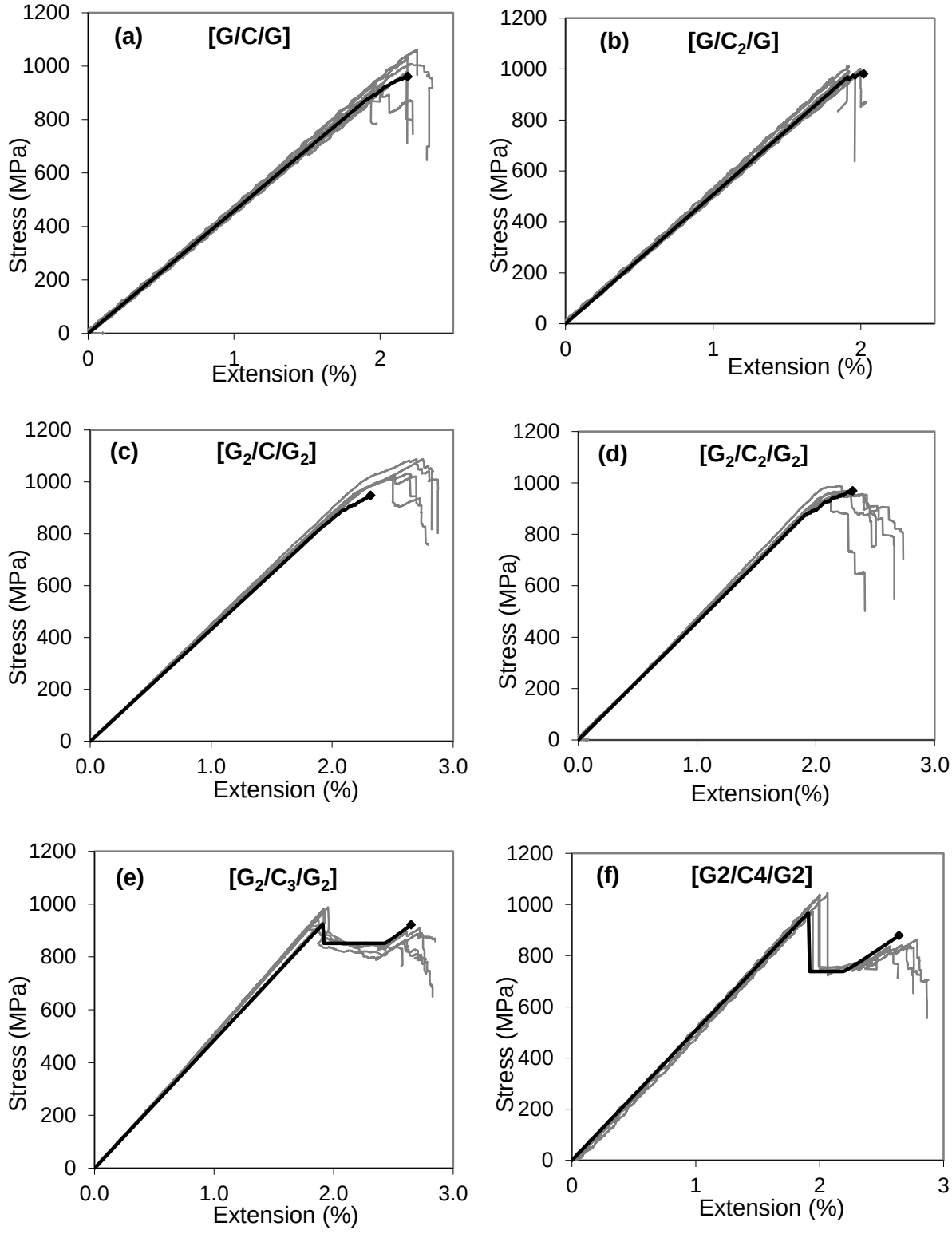

Figure 10- (a-f) Comparison of FE stress-extension curves of laminates [G/C_m/G] and [G_2/C_n/G_2] (m=1, 2 and n=1-4) against experimental results

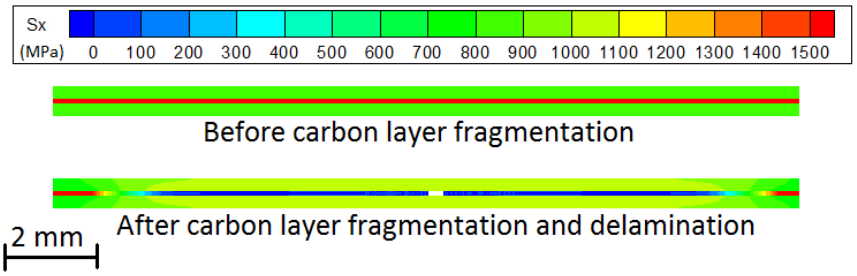

Figure 11- The stress distribution just before carbon layer fracture and after unstable delamination in the laminate [$G_2/C_3/G_2$]

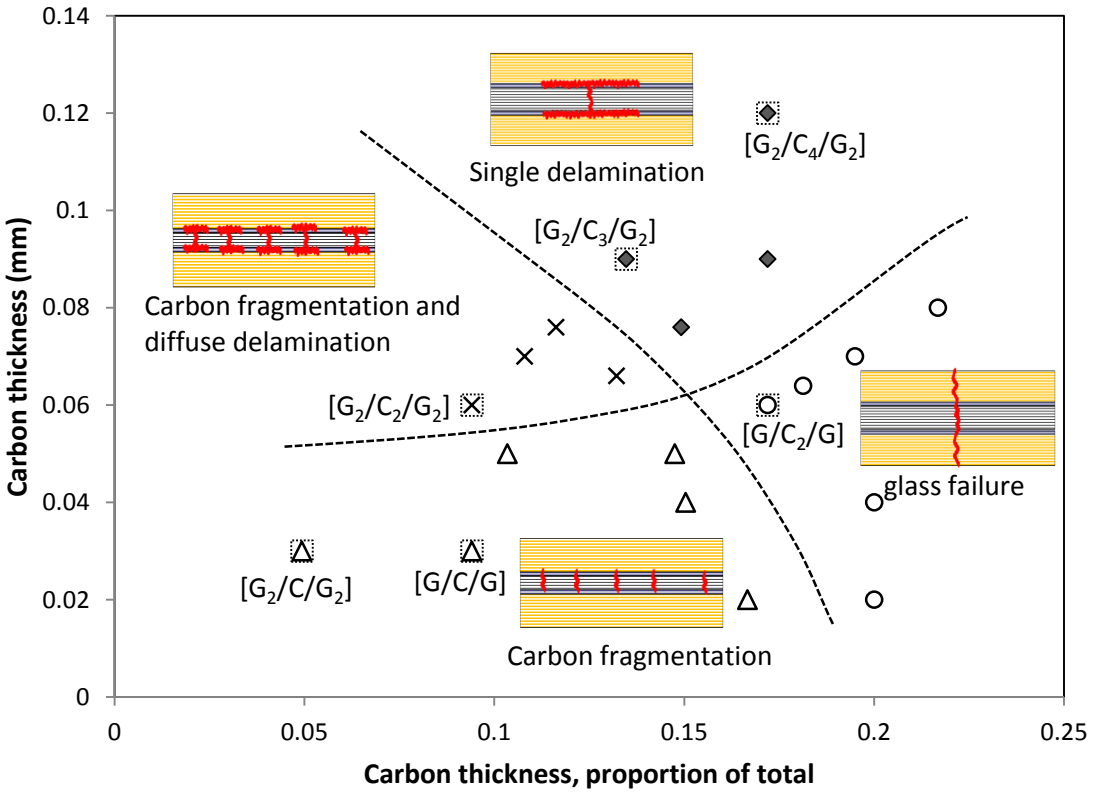

Figure 12- Categorisation of different damage modes as a function of absolute and relative thickness of carbon layers